

# Ag/Cu(111) surface structure and metal epitaxy by impact-collision ion-scattering spectroscopy and scanning tunneling microscopy

Kenji Umezawa\* and Shigemitsu Nakanishi

*Department of Materials Sciences, Osaka Prefecture University, Sakai, Osaka 599-8531, Japan*

Masamichi Yoshimura, Kaoru Ojima, and Kazuyuki Ueda  
*Toyota Technological Institute, Hisakata, Tempaku-ku, Nagoya 468-8511, Japan*

Walter M. Gibson

*Department of Physics, State University of New York at Albany, 1400 Washington Avenue, Albany, New York 12222*

(Received 31 July 2000; published 22 December 2000)

We have investigated the growth of 3 monolayers (ML) of Ag on Cu(111) for substrate temperatures from 170 through 640 K by using time of flight-impact collision ion scattering spectroscopy (TOF-ICISS). Also, scanning tunneling microscopy (STM) topographs were taken after the deposition of 0.8 ML of Ag atoms at room temperature (RT). We observed that for deposition of Ag at substrate temperatures above 300 K, two different types of epitaxial growth exist:  $\text{Ag}[11\bar{2}]\parallel\text{Cu}[11\bar{2}]$  (type-*n*) and  $\text{Ag}[\bar{1}12]\parallel\text{Cu}[11\bar{2}]$  (type-*r*). The growth modes of the Ag thin films on Cu(111) surfaces depend strongly on the temperature during deposition with the Ag(111) planes having a preferred orientation of either type-*n* growth mode or type-*r* growth mode as a function of the Cu substrate temperature. A part of the first-layer Cu atoms (20% of the surface) is displaced at low Ag coverage, where the stacking changes abruptly from fcc to hcp sites because of the Ag atom deposition at 603 K. The STM image of the Ag coverage of 0.8 ML showed a periodic array of triangular misfit dislocation loops at the deposition temperature of RT. The triangular shape in a localized region where the stacking {Ag—Cu (A)—Cu (B)—Cu (C)} is replaced by {Ag—Cu (C)—Cu (B)—Cu (C)} in the first substrate plane. At 603 K, surface alloying of the Ag—Cu system was confirmed for Ag coverage below 0.15 ML. The experimental results concerning Ag/Cu(111) show many similarities to those in the previous study of Au/Ni(111). This would suggest that observed oscillations in the growth mode, dependent on the substrate temperature during deposition, may be a general phenomenon on solid surfaces, in cases of large misfit since it has now been seen for both Au/Ni(111) and Ag/Cu(111) systems. Furthermore, Cu atoms deposited on the Ag/Cu(111) system form islands with the same orientation of Ag(111) planes. The Cu atoms undergo surface diffusion at room temperature in the direction of type-*n* domains for both type-*r* and type-*n* modes Ag substrates.

DOI: 10.1103/PhysRevB.63.035402

PACS number(s): 68.35.Bs, 81.15.-z

## I. INTRODUCTION

In recent years, considerable progress has been achieved in the understanding of how atomic processes contribute to thin film growth. Understanding and controlling growth morphologies requires detailed knowledge of microscopic processes for both fundamental and technological reasons. Recent advances in epitaxial growth techniques have greatly expanded our capabilities to grow artificially structured materials, which can not be found in nature.<sup>1</sup> Epitaxial growth can produce films with significant strain, or, in some cases, a crystal lattice structure different from the bulk material. Especially, heteroepitaxy often involves lattice mismatch between the deposited film and the substrate that will produce strain at the interface between the deposited film and the substrate. It is also well known that different growth modes can result from changes in the substrate temperature as well as the deposition rate.<sup>2</sup>

Large difference in the lattice spacing between the deposit and the substrate tends to lead to an overlayer of unique structure. The Ag/Cu(111) system can be considered as representative of the case: a large deposition atom and small substrate atom for two species which are almost completely

immiscible in the bulk.<sup>3</sup> The Ag/Cu(111) combination has a large lattice mismatch (13%); the nearest neighbor distances of bulk Ag(111) and Cu(111) are 2.89 Å and 2.56 Å, respectively.<sup>4</sup> The Ag/Cu(111) system is very similar to the Au/Ni(111) system. The lattice mismatch between Au and Ni is 16%; the nearest neighbor distances of bulk Au(111) and Ni(111) are 2.88 Å and 2.49 Å, respectively. Elemental Au-Ni is also immiscible in the bulk. In both cases, low energy electron diffraction (LEED) patterns display (9×9) structures at a coverage of 1 ML.<sup>5-7</sup> The (9×9) structure is explained considering the bulk lattice parameter of deposited and substrate atoms. The lattice parameters are almost commensurate with the ratio  $d(\text{Ag})/d(\text{Cu})$  and  $d(\text{Au})/d(\text{Ni})$  close to 9/8, respectively. In such incommensurate systems, many atoms occupy “less favorable positions” with respect to the substrate, and one can expect a strong process of relaxation. In a previous study, we investigated the surface structure and metal epitaxy for the Au/Ni(111) system by using impact collision ion scattering spectroscopy (ICISS).<sup>8</sup> We showed that two simple, symmetric growth modes dominate the ordered heteroepitaxy and the relative abundance of these two modes exhibits a striking and previously unob-

served oscillatory dependence on the substrate temperature during deposition. The deposition of Au on Ni(111) gave new insight on metal/metal heteroepitaxy growth mechanisms. As a continuation of that work,<sup>8</sup> we now report on and discuss in detail the heteroepitaxial growth behavior for Ag films [ $\sim 3$  monolayers (ML)] on Cu(111) surfaces using time-of-flight impact collision ion beam scattering spectroscopy (TOF-ICISS). In addition, scanning tunneling microscopy (STM) images were obtained for the Ag/Cu(111) system after the deposition of 0.8 ML Ag atoms at room temperature (RT).

Low kiloelectron-volt energy ion beam scattering with time-of-flight (TOF) detection is well established for analyzing both the atomic composition and the surface structure of single crystals.<sup>9</sup> The STM technique provides an unprecedented microscopic view of activated processes taking place on surfaces. In many ways, the TOF-ICISS and the STM measurements are complementary in studies of the topmost layers of simple crystals and thin film heteroepitaxy systems. Both methods reveal new aspects in the adsorbate system Ag/Cu(111). The experimental results for Ag/Cu(111) show many similarities to those of the previous study of Au/Ni(111).<sup>7,8</sup> This indicates that the remarkable oscillatory dependence of the growth mode on substrate temperatures observed for Au/Ni(111) is not confined to that system but is more general, since it is present for both the Au/Ni(111) and Ag/Cu(111) systems.

Furthermore, the surface structures of Cu/Ag superlattice films are also of fundamental and technological interest. We have investigated the surface structures of Cu/Ag/Cu(111) systems with ICISS. Cu atoms were deposited on samples exhibiting each of the two different modes of the Ag/Cu(111) systems at RT. One was a preferred orientation of type-*r*, and the other was a preferred orientation of type-*n*.

In addition, the experimental values of the incident ion scattering critical angle, defined as the angle where the intensity curve attains the 70% maximum<sup>10</sup> has been used to investigate the out-of-plane displacement of Ag adatoms at low coverage. A Thomas-Fermi-Molière (TFM) potential was used with the screening length proposed by Firsov.<sup>11,12</sup> The factor used for the Firsov length were taken as 0.85 for Ag atoms and 0.75 for Cu atoms in the computer simulations analysis.<sup>13</sup>

## II. EXPERIMENTAL PROCEDURES

Two different experimental procedures, TOF-ICISS and STM, were used. The experimental technique for TOF-ICISS has been described in detail in previous publications.<sup>8,14,15</sup> An outline is given in this report. The experimental procedures described here were performed in an ultrahigh vacuum chamber with LEED Auger electron spectroscopy (AES), and TOF-ICISS facilities. The base pressure was maintained below  $5 \times 10^{-9}$  Pa. A Cu(111) ( $\phi = 15 \text{ mm} \times 1 \text{ mm}$  thickness) single crystal was mounted on a standard *xyz* manipulator and cleaned *in situ* by repeated cycles of 500-eV Ar<sup>+</sup> bombardment followed by annealing at 770 °C to remove the surface damage until no contamination could be detected by

using AES and ICISS. The clean crystal showed a sharp unreconstructed  $1 \times 1$  LEED pattern. We also used ICISS measurements to ensure that the Cu crystal is not twinned. Twinning is easily seen in ICISS polar scans. After depositing Ag at a coverage of about 1.0 ML at RT, the LEED pattern displayed a  $9 \times 9$  LEED pattern with respect to the underlying Cu lattice. The sample temperature was monitored using a chromel-alumel thermocouple tightly attached on the front side of the Cu(111) sample. Ag of 99.999% purity was evaporated at a rate of about 0.1 ML/min onto the Cu(111) crystal to a coverage of 3 ML at various substrate temperatures from 170 through 640 K. The ICISS spectra were taken by chopping the primary 2-keV <sup>20</sup>Ne<sup>+</sup> ion beam and measuring the 180° backward scattered particle intensity with a microchannel plate (MCP) that was coaxially mounted along the primary drift tube. Following Ag deposition at specified substrate temperatures, the ICISS measurements were performed at a substrate temperature of about 300 K. Ag and Cu TOF spectra were well resolved as a function of Ag coverage. Polar scans were performed from  $-85^\circ$  to  $+85^\circ$  in  $2^\circ$  increments with a pulsed beam current of  $3 \sim 5$  pA. Azimuth scans were performed from  $-72^\circ$  to  $+72^\circ$  in  $3^\circ$  increments as well. The time required for a complete scan was typically 40 min, resulting in a total dose of  $\sim 5 \times 10^{10}$  ions/cm<sup>2</sup>.

The STM experiments were carried out in an ultrahigh vacuum chamber at Toyota Technological Institute.<sup>16</sup> The base pressure was maintained below  $2 \times 10^{-8}$  Pa. The Cu(111) single crystal used was  $2 \text{ mm} \times 7 \text{ mm} \times 1 \text{ mm}$  thickness and was cleaned *in situ* by repeated cycles of 1-keV Ar<sup>+</sup> bombardment followed by annealing at 780 °C until clean surfaces were confirmed by STM observations at room temperature. Ag of 99.999% purity was evaporated at a rate of about  $2.7 \times 10^{-2}$  ML/min onto the Cu(111) crystal to a coverage of 3 ML at about 300 K. The STM observations were performed at room temperature for various coverages by using electrochemically sharpened tungsten tips. For both ICISS and STM measurements, the Ag evaporation rates were verified by Rutherford backscattering spectroscopy (RBS) measurements using 2-MeV <sup>4</sup>He<sup>+</sup> ions produced by a 4 MV Dynamitron accelerator facility at State University of New York at Albany. A silicon surface barrier detector (SSBD) with a 31.1 m sr. solid angle was located at  $164^\circ$  from the incident beam for these measurements. A coverage of 1 ML corresponds to the Cu(111) surface density of  $1.77 \times 10^{15}$  atoms/cm<sup>2</sup>.

In a separate series of measurements, Cu atoms were deposited on two different kinds of Ag/Cu(111) surfaces at RT. One Ag(111) structure had a preferred orientation of type-*r* and the other type-*n*. The type-*r* structure was produced by depositing 3 ML of Ag atoms on the Cu(111) substrate at 303 K. The type-*n* structure was produced with the same Ag coverage on the Cu(111) substrate at 563 K. As will be shown, these conditions correspond to maxima of type-*r* and type-*n* orientations, respectively. The evaporation rate of Cu atoms was  $1.5 \times 10^{-2}$  ML/min in the system of Cu/Ag/Cu(111).

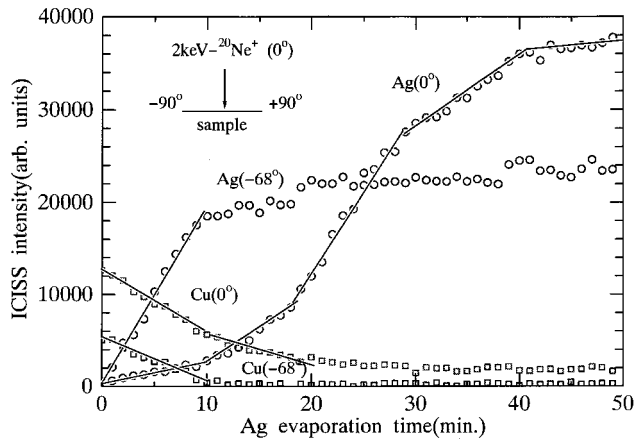


FIG. 1. ICISS peak intensities as a function of Ag evaporation time at specific polar angles of  $-68^\circ$  and  $0^\circ$ . The ICISS intensities were taken by 2-keV  $^{20}\text{Ne}^+$  ions backscattered from the sample along a  $[11\bar{2}]$  azimuth.

### III. RESULTS AND DISCUSSION

#### A. Growth mode dependence on substrate temperature during deposition for Ag/Cu(111)

It is well known that heteroepitaxial growth mode of thin films on solid surfaces can be classified into three different types: Volmer-Weber (VM) mode (island growth), Frank-van der Merwe (FM) mode (layer-by-layer growth) and Stranski-Krastanov (SK) mode (layer+island growth). Multiple scattering effects of low energy ion beams are particularly pronounced in TOF-ICISS, giving rise to focusing effects in which the flux density of primary beams impinging on an atom is strongly enhanced at several specific angles of the incident ion beams. Flux enhancement due to focusing effects can be applied for atomic structure analysis of the topmost surface layers. When the direction of the incident ion beam is fixed at a focusing angle for the epitaxial overlayers, the rate of change of the scattered signal intensity changes at the completion of each two-dimensional (2D) layer coverage. Focusing effects are strongest when the overlayer has the same crystallographic orientation as the substrate. Conversely, such effects are small or absent for disordered or amorphous overlayers. Figure 1 shows ICISS peak intensity as a function of Ag evaporation time for the specific polar angles of  $-68^\circ$  and  $0^\circ$ . The break points of Ag intensities at  $0^\circ$  appears at about every 10 min ( $\theta=1$ ), which corresponds to the time necessary to deposit one ML. This clearly shows that the growth occurs in a FM mode fashion up to at least five layers. Meanwhile, the slope of the Cu intensity also changes at the same coverage (Ag deposition time of 10 min). This is shown for polar angles of  $0^\circ$  and  $-68^\circ$ , respectively. The ICISS intensities at a polar angle of  $-68^\circ$  come from the outermost layer of Ag and Cu atoms due to focusing effects. The polar angle of  $0^\circ$  corresponds to primary beams which perpendicularly strike the sample surface as shown in the insert of Fig. 1. The Cu ICISS signal going to zero at this angle at the deposition time of 10 min shows that the topmost layer of Cu atoms were completely

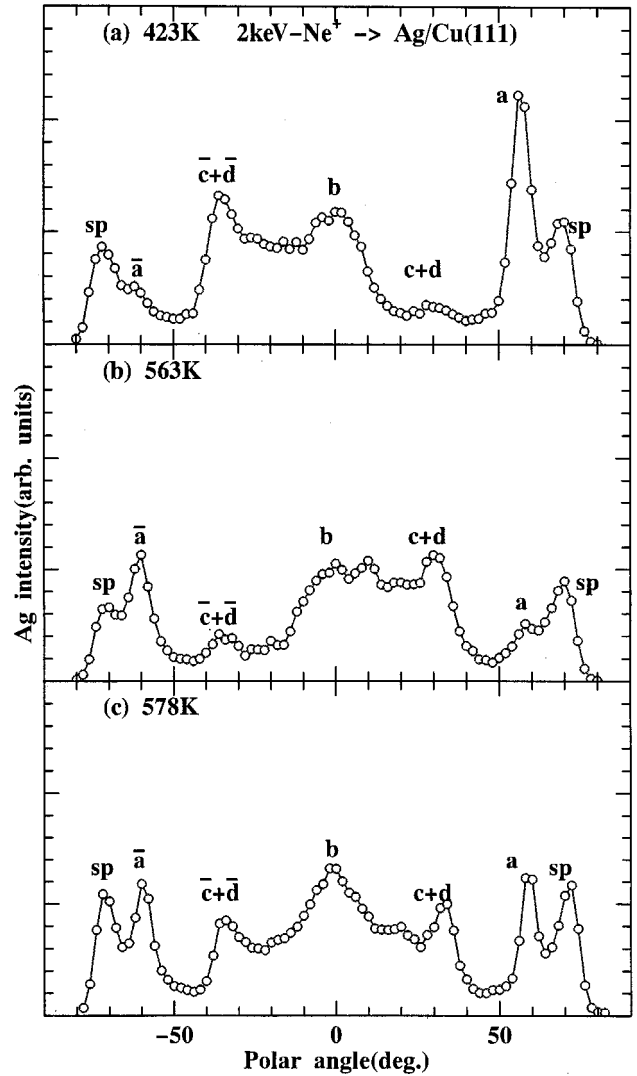


FIG. 2. A series of TOF-ICISS polar scans for 2-keV  $^{20}\text{Ne}^+$  ions backscattered from Ag atoms at coverage of 3 ML along a  $[11\bar{2}]$  azimuth following Ag deposition at different substrate temperatures. The polar angle was measured from the surface of the specimen. As discussed in the text, in (a) a normal growth mode (type- $n$ ) is dominant and in (b) a reverse growth mode is dominant (type- $r$ ). The two growth modes are equally populated in (c).

covered by 1.0 ML of Ag atoms. The features shown in Fig. 1 were found to be reproducible over many experiments.

Figure 2 shows a typical series of ICISS polar angle scans along the  $[11\bar{2}]$  azimuths for 2-keV  $^{20}\text{Ne}^+$  scattered from 3 ML of Ag atoms deposited at different substrate temperatures onto Cu(111). In Fig. 2(a) the Ag intensity at around  $-25^\circ$  is strong, and the Ag intensity at  $+25^\circ$  is weak, whereas Fig. 2(b) shows the opposite behavior. In Fig. 2(c) the Ag intensity is symmetric around the polar angle of  $0^\circ$ . These results clearly show that the spectra of the polar angle scans change remarkably depending on the substrate temperature during Ag deposition. In each case the ICISS measurements were made at RT. This result is very similar to that found previously for the Au/Ni(111) system.<sup>8</sup> As discussed in detail for the Au/Ni(111) system, peaks in the polar

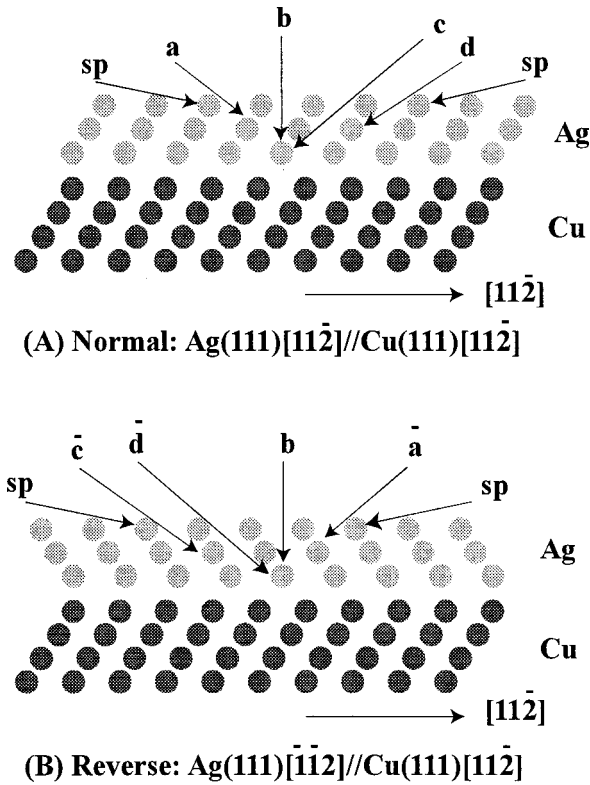


FIG. 3. Side view of Ag(111) planes for heteroepitaxial growth on Cu(111) substrates. (A) and (B) show type-*n* and type-*r* domains, respectively. The symbols “a,” “b,” “c,” “d,” “sp,” “ $\bar{a}$ ,” “ $\bar{c}$ ,” and “ $\bar{d}$ ” show positions where focusing effects are expected to appear for the two different domain types.

scan are associated with scattering from atoms at specific depths for beams incident in different directions as indicated schematically in Fig. 3 for two different growth modes. When the two modes are present in equal amounts the polar scan is symmetric around the polar angle of 0° as shown in Fig. 2(c).

The ICISS polar scan spectra result from both interaction of an atom with the enhanced flux at the edge of a shadow cone of another atom and from the enhanced flux at the edge of a blocking cone. Therefore, if the flux at the edge of each shadow and blocking cone in a particular model of surface structure is calculated, the ICISS polar scan spectra can be constructed by assuming the flux distribution from each atom pair that contribute to the particular model of surface structure. From simulation calculations we can explain all of the observed peaks in scattering of 2-keV  $^{20}\text{Ne}^+$  beams for the Ag atoms in several specific incident directions. The simulations are based on the three-dimensional cross section for ions that scatter sequentially and classically from two atoms.

Figure 3 shows side views of two different types of Ag(111) epitaxial growth mode on Cu(111) substrates, e.g., Ag[112]||Cu[112] (normal: type-*n*) and Ag[112]||Cu[112] (reverse: type-*r*). That is to say, the type-*n* film has a parallel orientation with respect to the Cu substrate, but the type-*r* film has an antiparallel orientation (a lattice orientation rotated 180°) with respect to the Cu substrate. In these figures, arrows show the directions of incident beams at particular

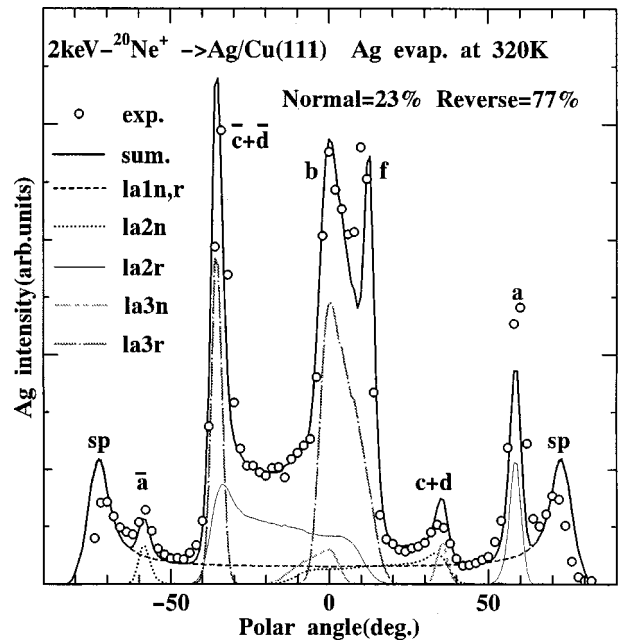


FIG. 4. Open circles show the TOF-ICISS polar scans for 2-keV  $^{20}\text{Ne}^+$  ions backscattered from Ag atoms at coverage of 3 ML along a [112] azimuth. The Ag deposition onto Cu(111) sample was carried out at 320 K. Computer simulations of the backscattered intensity are shown as solid and dashed curves. The ratio of type-*n* vs type-*r* was chosen to be 23% and 77% for the simulations. The solid line shown by the symbol of “sum” is the total calculated intensities from first through third layers of Ag atoms. The symbol “la1n,r” shows the calculated intensities coming from first-layer Ag atoms. The symbols “la2n” and “la2r” show the calculated intensities coming from second-layer Ag atoms of type-*n* and type-*r*, respectively. The symbols “la3n” and “la3r” show the calculated intensities coming from third-layer Ag atoms of type-*n* and type-*r*, respectively.

angles. For example, the arrow labeled “b” indicates that the incident beam hits the atoms perpendicular to the sample surface. It corresponds to the polar angle of 0° in Figs. 2 and 4. We divide the observed peaks shown in Figs. 2 and 4 into two groups: one group labeled a, b, c, d, and sp, and another  $\bar{a}$ ,  $\bar{b}$ ,  $\bar{c}$ ,  $\bar{d}$ , and sp as shown in Fig. 3. The first group is called the normal growth mode (type-*n*) and the second is called the reverse growth mode (type-*r*) with respect to the substrate Cu atoms. Simulations were performed depending on the ratio between the normal and reverse modes as shown in Fig. 4. Circles, solid lines, and dotted lines show the experimental results and simulation results, respectively. Simulation results for the spectrum shown in Fig. 4 show that for this case, the type-*n* versus type-*r* mode abundances are 23% and 77%, respectively, at 320 K. We call attention to the Ag signals at  $\pm 25^\circ$ . Because the Ag signals at  $\pm 25^\circ$  mainly come from scattering from the second layer of Ag atoms, either type-*n* or type-*r*, e.g., plus scattering from the first layer of Ag atoms. However, the signal intensity from the first layer of Ag atoms is flat for all samples and merely provides a flat background in the spectra. Other peak signals labeled “ $\bar{c}+\bar{d}$ ” and “c+d” come from the sum of the second and third layers of Ag atoms. In particular, for these peaks, focusing effects

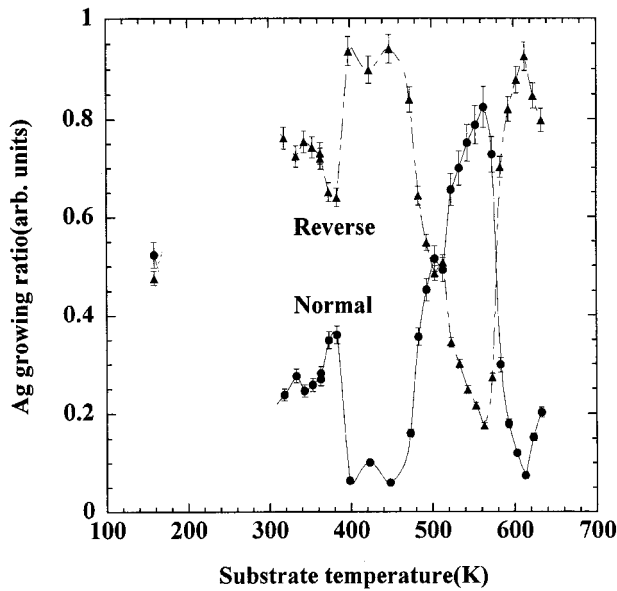


FIG. 5. Variation of growth ratio for type-*n* and type-*r* Ag growth modes as a function of growth temperature during Ag deposition.

coming from the third layer of Ag atoms are especially strong. In practice, the second layer of Ag atoms shows the orientation as a function of the Cu substrate temperature during Ag deposition. The experimental polar scans were fitted with linear combination of simulated scans for the two growth modes. The fits show that there are no other significant overlayer structures present.

The ratio of each mode determined from these fits as a function of substrate temperature during the Ag deposition is shown in Fig. 5. This figure shows strong oscillations in the growth mode, dependent on the substrate temperature. One can see that Ag(111) planes grow as mixed domain of 50% each of type-*n* and type-*r* at specific growth temperatures of 500 and 580 K. The ICISS spectra of polar angle scans were identical at these temperatures to that already shown in Fig. 2(c). Between 380–500 K and >580 K, Ag(111) planes grown on the substrate have a preferred orientation of type-*r* domains. On the other hand, between 500–580 K, the type-*n* domains are preferred as a growth mode. After 3 ML of Ag atoms were grown with a preferred orientation at a certain substrate temperature, the ratio of growth mode was frozen and independent of subsequent changes in substrate temperatures. This oscillation behavior is quite similar to that in the Au/Ni(111) system.<sup>8</sup> The mechanism underlying this dramatic oscillation behavior is not understood. However, it is sufficiently general to encompass Ag/Cu(111) and Au/Ni(111) and may also apply to other systems as well.

### B. Adatom-induced reconstruction of the Cu substrate for Ag/Cu(111) at low coverage

Figure 6 shows a series of ICISS polar angle scans for Ne scattered from Ag and Cu atoms along the  $[11\bar{2}]$  azimuth for various deposition times of Ag on a Cu(111) sample up to 3 ML at 320 K. The characteristics of two different domains in

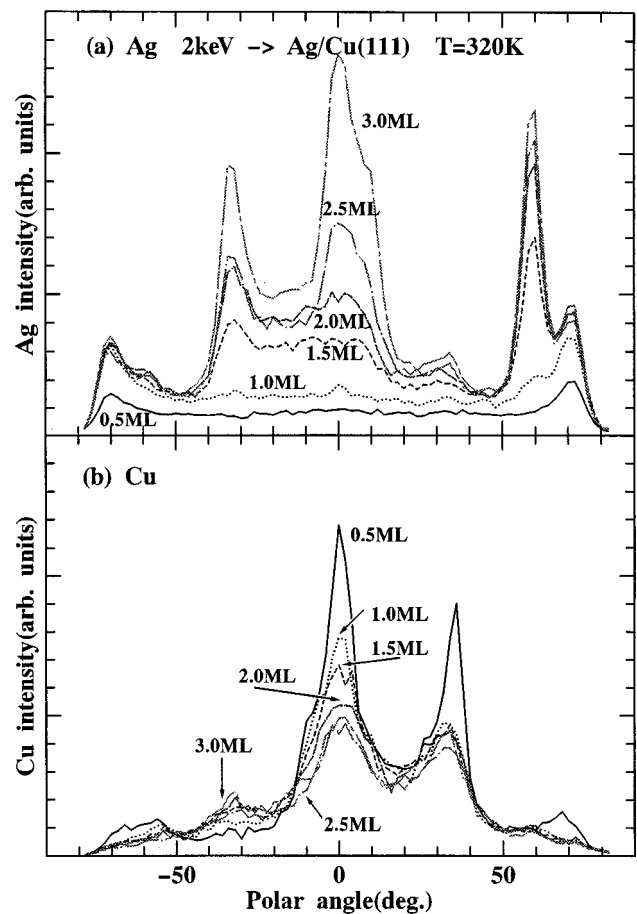


FIG. 6. A series of TOF-ICISS polar scans along the  $[11\bar{2}]$  azimuth for various times of Ag deposition on a Cu(111) sample at 603 K (a) Ag intensity and (b) Cu intensity are shown as a function of the polar angle of incidence of 2-keV Ne<sup>+</sup> ions.

the initial stage of Ag growth can be seen from signal peaks at about  $\pm 32^\circ$ , since they exhibit the feature signals coming from two domains. As shown in Figs. 3 and 4, the peaks at  $+32^\circ$  come from Ne scattered at the specific incident angles of  $\bar{c}$  and  $\bar{d}$  (type-*n*). The peaks at  $-32^\circ$  in Fig. 6(a) come from Ne scattered at the incident angles of  $c$  and  $d$  (type-*r*). As noted previously, first-layer Ag atoms do not show either type-*n* or type-*r* difference. The intensity of Cu signals for each polar angle scan becomes weaker with increasing amount of Ag deposition as shown in Fig. 6(b). However, a peak arising from scattering of Ne from Cu at about  $-32^\circ$  is observable with Ag evaporation. No peak at  $-32^\circ$  along the  $[11\bar{2}]$  azimuth was observed from a clean Cu(111) sample, as shown in Fig. 7. Simulation analysis suggests that some of the first-layer Cu atoms were moved and localized in part of the surface where the stacking changed abruptly from ABC to ABA (hcp sites: corresponding to 1.4 Å displacement). The peak signals at about  $-32^\circ$  for both 320 and 560 K show that first-layer substrate Cu atoms shifted from fcc to hcp sites due to the Ag atom deposition allowing second-layer Cu atoms to contribute to the scattering at this specific polar angle due to focusing effects. This peak at  $-32^\circ$  was not observed for a clean Cu(111) surface. However, one can

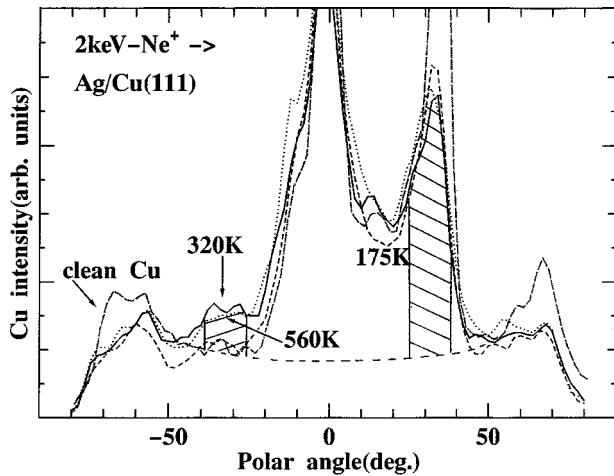


FIG. 7. Cu intensity taken at RT as a function of polar angle along the  $[11\bar{2}]$  azimuth after depositing 1 ML of Ag at substrate temperature of 175, 320, and 560 K. In addition, clean Cu(111) signals were taken at RT. Hatched areas at  $+32^\circ$  and  $-32^\circ$  mainly come from second-layer Cu atoms. In particular, peak signals at  $-32^\circ$  are due to stacking changes from fcc to hcp sites in first-layer Cu atoms. Dashed lines show the Cu intensity expected from scattering from first-layer Cu atoms.

see that the Cu intensity when covered by 1 ML of Ag at 175 K at  $-32^\circ$  has the same height as that of clean Cu(111). This suggests that local stacking faults due to shifting of surface-layer Cu atoms do not take place on a cold Cu(111) surface ( $T=175$  K).

The number of Cu atoms shifted from face-centered-cubic (fcc) to hexagonal-close-packed (hcp) sites at 320 and 560 K can be estimated by comparison of the signal areas (hatched areas) at about  $+32^\circ$  and  $-32^\circ$ . The Cu signal intensities at these specific polar angles have almost the same heights at both deposition temperatures. It is noticed that the Cu intensity shown by dashed lines mainly comes from first-layer Cu atoms. We conclude that about 20% of first-layer Cu atoms shift to hcp sites when 1 ML of Ag atoms is deposited on the substrate at 320 and 560 K. Moreover, the number of the Cu atoms shifted from fcc to hcp sites did not increase with Ag coverage after 1 ML deposition. A STM topograph is shown in Fig. 8 after deposition of 0.8 ML Ag atom at RT. The STM topograph ( $1230 \times 1230 \text{ \AA}^2$ ) of Ag adsorbed onto Cu at RT reveals a periodic triangular structure. This STM picture was recorded at 0.22 V and 0.68 nA tunneling current. The array of triangular pits has the same angular orientation. In this image a few atoms exist in the center. The line scan (white color) in the STM image illustrates the details of the atomic corrugation in a triangle and the corrugation is about 0.5 Å. The distance between the center of two neighboring triangles is about nine times the interatomic distance in the Ag(111) plane. The STM image at a coverage of 0.8 ML Ag shown here is quite similar to those observed by the same technique for the Au on Ni(111) system,<sup>6</sup> although our STM image has lower resolution than that obtained for Au/Ni(111). In the previous Au/Ni(111) study the authors suggested the following scenario: The triangular structures appear close to the top positions relative to the underlying Ni

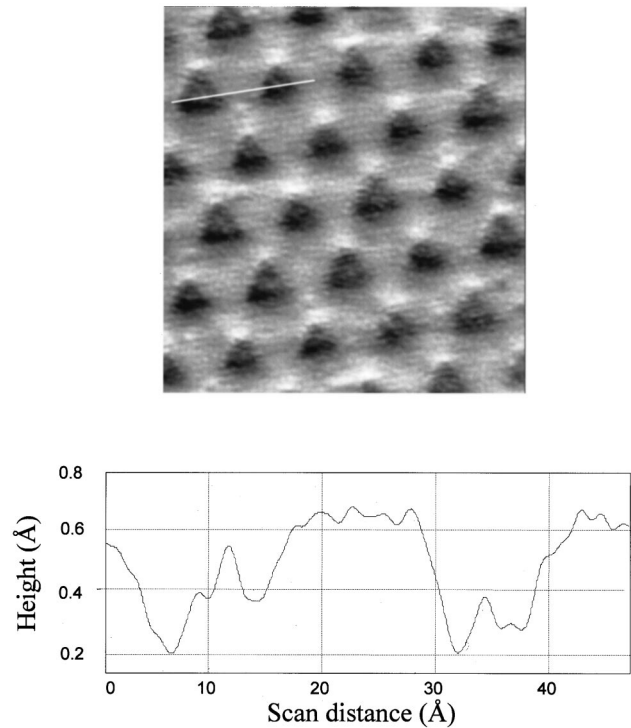


FIG. 8. STM image ( $1230 \text{ \AA} \times 1230 \text{ \AA}$ ) after deposition of 0.8 ML Ag at RT revealing a network of triangles. The line scans indicated by a white line show the details of the atomic corrugation in a triangle.

layer. The squeezed-out Ni atoms from the top substrate allow some substrate Ni atoms to shift from fcc to hcp sites, and Au atoms are then situated in the center of triangular structures. A single monolayer of Au on Ni(111) results in an ordered array of triangular misfit dislocation loops. Thus, it could be understood that the triangular structures are formed due to the misfit of the Ag overlayer and Cu substrate. We estimate that about 20% of first-layer Cu atoms shift from fcc to hcp sites based on ICISS results could be explained by a similar model. Meunier and co-workers have suggested that creation of vacancies in the first Cu substrate layer can be explained from a thermodynamical point of view.<sup>3</sup> Triangular misfit dislocation loops are due to the relaxation of the interface stress between the Ag adlayer and first Cu layer. Removed Cu atoms probably situated at some substrate step edges. A triangular structure indicated by the STM image is illustrated in Fig. 9. In this model, five Cu atoms are removed from a  $9 \times 9$  Cu(111) surface during the Ag deposition. This allows 10 Cu atoms to shift from fcc to hcp sites. That is to say, the fcc-to-hcp shift of the Cu atoms forms local stacking faults and offers more stable threefold hollow sites for the overlayer Ag atoms. The ratio of Cu atoms occupying hcp sites to fcc sites is 15% in this 2D domain. In fact, the number of Cu atoms removed from the first layer depends on the size of the stacking faults. If six Cu vacancies exist, 24% of Cu atoms shift from fcc to hcp sites.

However, as discussed above and shown in Fig. 7, the ratio of first-layer Cu atoms in hcp sites (Cu signals at  $-32^\circ$ ) does not increase at 175 K. The Cu intensity at this angle has

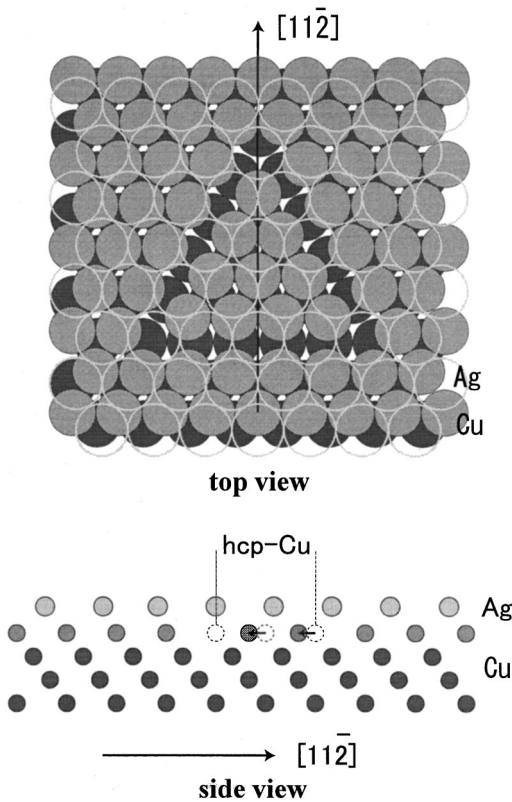


FIG. 9. Top view shows a model of a triangular misfit dislocation. The side view shows the fcc to hcp sites in first layer Cu atoms because of Ag deposition. Black circles show first-layer Cu atoms and gray circles show second-, third- and fourth-layer Cu atoms.

the same height as that of clean Cu(111) along the  $[11\bar{2}]$  azimuth, when covered by 1 ML of Ag atoms. Indicating that local stacking faults due to shifting of surface-layer Cu atoms does not take place at a substrate temperature of 175 K.

Information about the registration between the Ag atoms and the Cu layer can be obtained from the position of the surface peak (sp) in the polar angle scan. This peak appears when the edge of the shadow cone from ions scattered from one Ag atom intercepts the adjacent Ag atom. Figure 10 shows the Ag intensity as a function of polar angles between  $-70^\circ$  and  $-80^\circ$  along a  $[11\bar{2}]$  azimuth. The Ag coverage was from 0.03 through 0.5 ML, and the substrate temperature during deposition was 603 K. The Ag-Ag spacing can be obtained by calculating the Ag shadow cone radius using an appropriate Thomas-Fermi (TF) atomic potential. The Ag intensities at a polar angle of  $-74^\circ$  as a function of Ag coverage are summarized in Fig. 11. The three different regions correspond to the formation of a surface alloy, a mixing zone (surface alloy and overlayer). A plot of the Ag scattering intensity as a function of Ag coverage has a change of slope at a coverage of 0.15 ML. This shows the presence of surface alloying below a coverage of 0.15 ML. For Ag deposition less than 0.15 ML the Ag intensity shows a common critical angle of  $77.5^\circ$  (corresponding to a glancing angle of  $12.5^\circ$  from the sample surface), indicating that the edge of the shadow cone for Cu atoms passes through the center of neighboring Ag atoms at a critical angle of  $12.5^\circ$ . From the

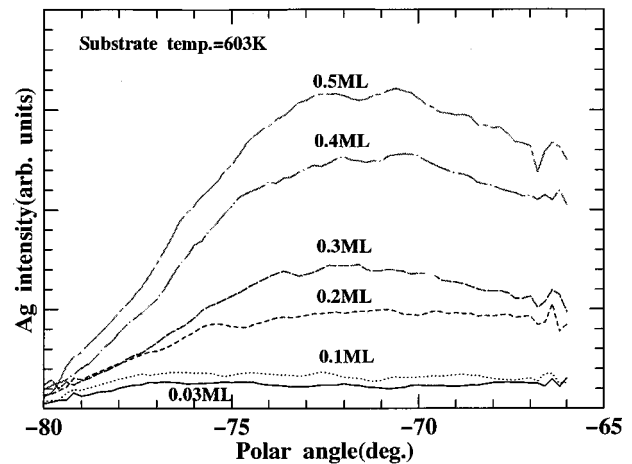


FIG. 10. Ag intensity as a function of polar angles between  $-70^\circ$  and  $-80^\circ$  along a  $[11\bar{2}]$  azimuth. The Ag coverage was from 0.03 through 0.7 ML, and the substrate temperature during deposition was 603 K.

shadow cone analysis, it was found that the Ag atoms displace first-layer Cu atoms and incorporate into first-layer Cu atoms with an outward displacement of  $0.4 \text{ \AA}$ , as shown schematically in Fig. 12(a). Surface alloying of the Ag-Cu system in the outermost surface layers apparently exists for Ag deposition below 0.15 ML, even though Ag is immiscible in the bulk at RT. Furthermore, the critical angle for the Ag atoms increases with increased Ag deposition. Eventually, the critical angles show a constant value of  $16^\circ$  when the Ag coverage was over 1 ML. At a critical angle of  $16^\circ$ , the Ag-Ag spacing thus obtained is  $5.0 \text{ \AA}$  along a  $[11\bar{2}]$  azimuth. This can be converted to a Ag nearest-neighbor distance of  $2.80 \text{ \AA}$ , which is slightly less than the Ag-Ag dis-

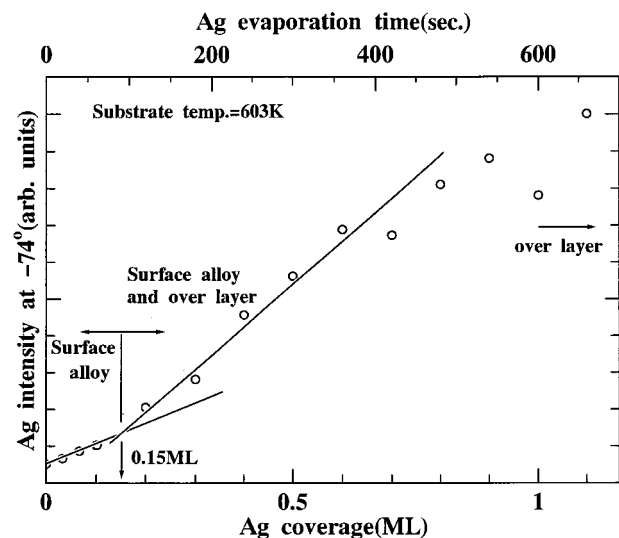


FIG. 11. Ag intensities at a polar angle of  $-74^\circ$  as a function of Ag coverage at a substrate temperature of 603 K. Three different structural conditions exist: surface alloy for Ag deposition below 0.15 ML; mixing zone of surface alloy and overlayer between 0.15 and 1 ML; and continuous overlayer for Ag coverage more than 1 ML.

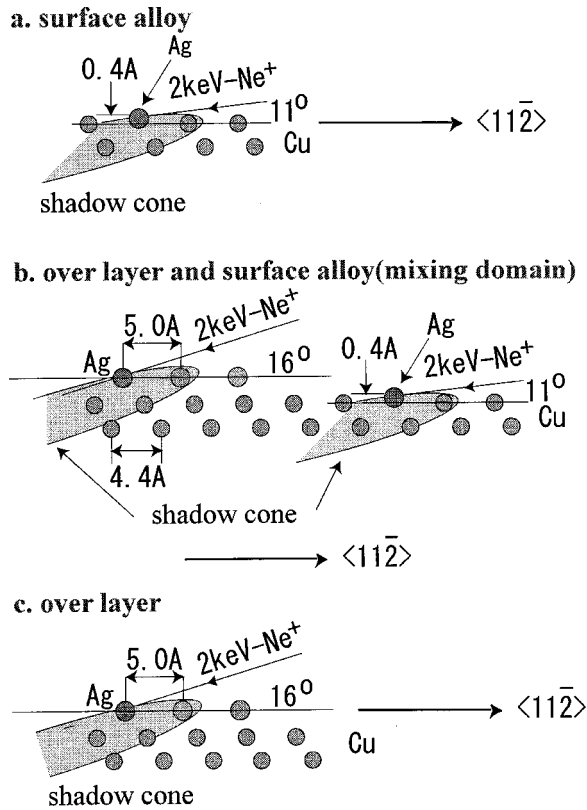


FIG. 12. Schematic illustration showing the shadow cone conditions: (a) surface alloy; (b) mixing zone (surface alloy and overlayer); (c) overlayer.

tance (2.89 Å) along a  $[\bar{1}10]$  azimuth in a bulk Ag crystal. This suggests that, at 1 ML coverage, the Ag layer is close to a simple overlayer structure, as shown in Fig. 12(c). However, the critical angle for Ag deposition at 170 K shows a constant value of  $16^\circ$  from the beginning of the deposition, again showing that surface alloying of the Ag-Cu system in the outermost surface layers does not take place at 170 K.

### C. Structural measurements for Cu/Ag/Cu(111)

We have also obtained experimental results for the Cu/Ag/Cu(111) system. Figure 13 shows a series of ICISS polar angle scans for ions backscattered from Ag and Cu atoms along the  $[11\bar{2}]$  azimuth. Cu atoms were deposited on the Ag/Cu(111) at a substrate temperature of 303 K. However, two different types of Ag(111) planes were completed on the Cu(111) substrate before the Cu deposition. One was a preferred orientation of type-*r* and the other was a preferred orientation of type-*n*. The type-*r* Ag(111) planes were grown at the substrate temperature of 303 K (mixed domains of 25% type-*n* and 75% type-*r*). Figures 13(a) and 13(b) correspond to this condition. The type-*n* Ag(111) planes were grown at a substrate temperature of 563 K (mixed domains of 80% type-*n* and 20% type-*r*). Figures 13(c) and 13(d) correspond to this condition. As shown in Figs. 13(a) and 13(c), the Ag intensities at  $-32^\circ$  (typical signals coming from the type-*r* domain) decrease more than those at  $+32^\circ$  (typical signals coming from the type-*n* domain) with in-

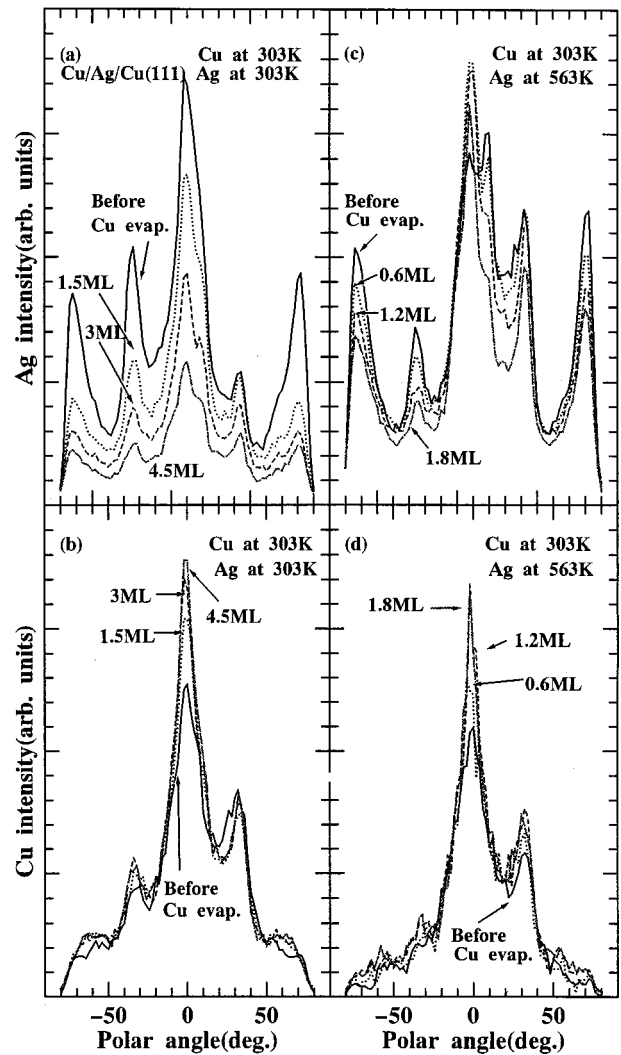


FIG. 13. A series of ICISS polar angle scans backscattered from Ag and Cu atoms along the  $[11\bar{2}]$  azimuth. Cu atoms were deposited onto two different type of Ag(111) planes at the substrate temperature of 303 K: (a) and (b) Ag atoms deposited at the substrate temperature of 303 K, (c) and (d) Ag atoms deposited at the substrate temperature of 563 K.

creased Cu deposition. In Fig. 13(b), the Cu intensities at  $-32^\circ$  become stronger with increasing Cu coverage. Meanwhile, the Cu intensities at  $+32^\circ$  have almost the same values independent of the Cu coverage. On the other hand, Fig. 13(d) shows that the Cu intensities at  $+32^\circ$  become stronger with increasing Cu coverage. This suggests that Cu films grow the same orientation with respect to the Ag(111) phase. In Figs. 13(a) and 13(b), type-*r* domains are more dominant than type-*n* domains. This is the reason why the Ag and Cu intensities at  $-32^\circ$  have some changes. In Figs. 13(c) and 13(d) this tendency is reversed. The Ag and Cu intensities at  $+32^\circ$  show changes, since type-*n* domains are more dominant than type-*r* domains. However, in either case (type-*r* dominant or type-*n* dominant), as shown in Figs. 13(a) and 13(c), the Ag intensities at  $-32^\circ$  decrease more than those at  $+32^\circ$  with increasing Cu deposition. This suggests that Cu atoms deposited on Ag(111) planes rapidly diffuse to type-*r*



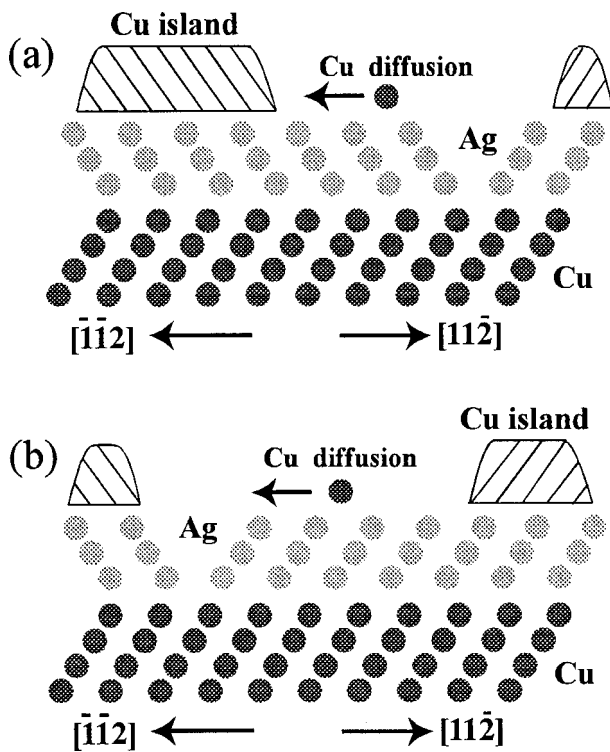


FIG. 14. Schematic illustration of the Cu growth modes derived for two different deposition conditions of Cu on Ag(111) planes: (a) deposition onto the type-*r* preferred domain, and (b) deposition onto the type-*n* preferred domain.

domains in both cases. We call attention to the Cu intensities at the polar angle of  $0^\circ$ . At this angle, the incidence direction of the primary 2-keV  $^{20}\text{Ne}^+$  beam is normal to the specimen surface. This incidence angle clearly observes the Cu planes on the Ag/Cu(111) system. At  $0^\circ$  incidence, the third layer of Cu atoms contribute strongly to the backscattering intensity because of focusing effects. The Cu signals at  $0^\circ$  mainly come from the third layer of Cu atoms on Ag(111) planes. In Fig. 13(a), the Ag intensity at  $-72^\circ$  (sp) decreases to about half of that before the Cu evaporation. This signal comes from the first layer of Ag atoms. This shows that about 50% of Ag atoms are covered by Cu atoms. However, the Cu signals at  $0^\circ$  in Fig. 13(b) clearly show scattering from the third layer Cu atoms. This means that about 1.5 ML of Cu atoms were deposited on Ag(111) planes and the Cu growth

process does not proceed layer-by-layer. If the Cu planes grew layer-by-layer, the Cu intensities at  $0^\circ$  would be strongly enhanced with increasing Cu deposition by the focusing effects of the ion beam. It is probable that the deposited Cu initially forms a 2D layer structure, and then surface diffusion of additional Cu atoms occurs rapidly, leading to coalescence into thick Cu islands. This is schematically shown in Fig. 14. In Figs. 14(a) and 14(b), Cu atoms were deposited on the Ag/Cu(111) phase at a substrate temperature of 303 K. The Ag/Cu(111) phase was completed at the substrate temperatures of 303 and 563 K, respectively, before Cu deposition. Ag(111) planes grown on the Cu substrate have a preferred orientation of type-*r* or type-*n*, respectively.

#### IV. CONCLUSIONS

We have investigated the growth of 3 ML of Ag on Cu(111) at substrate temperatures from 170 through 640 K by using TOF-ICISS. Also, STM topographs were taken after deposition of 0.8 ML Ag atoms at RT. We show that above a 300 K substrate temperature during Ag deposition, two different types of epitaxial growth exist: Ag $[\bar{1}\bar{1}\bar{2}]$ ||Cu $[\bar{1}\bar{1}\bar{2}]$  (type-*n*) and Ag $[\bar{1}\bar{1}\bar{2}]$ ||Cu $[\bar{1}\bar{1}\bar{2}]$  (type-*r*). The growth modes of the Ag thin films on Cu(111) surfaces depend strongly on the substrate temperature during deposition. For deposition of Ag at 603 K, a part of the first-layer Cu atoms (20% of the surface) is displaced at low Ag coverage, where the stacking changes abruptly from fcc to hcp sites because of the Ag atom deposition. STM images of the Ag coverage of 0.8 ML at RT showed a periodic array of triangular misfit dislocation loops. The triangular shape is a localized region where the stacking {Ag—Cu (A)—Cu (B)—Cu (C)} is replaced by {Ag—Cu (C)—Cu (B)—Cu (C)} in the first substrate plane. At 603 K, surface alloying of the Ag-Cu system was confirmed for Ag coverage below 0.15 ML, and the outward displacement of the Ag atoms was found to be 0.4 Å with respect to first-layer Cu atoms. The amount of surface alloying decreased with increasing Ag coverage, becoming unobservable at 1 ML. The Ag layer is close to a simple overlayer structure at this coverage. Furthermore, Cu atoms deposited on the Ag/Cu(111) system form islands with the same orientation as Ag(111) planes. The Cu atoms diffuse in the direction of a type-*n* domain for deposition on both type-*r* and type-*n* Ag growth modes, forming thick Cu islands.

\*Corresponding author: Fax: +81-722-54-9719; Email address: umezawa@ms.cias.osakafu-u.ac.jp

<sup>1</sup> *Initial Stages of Epitaxial Growth*, edited by R. Hull, J. M. Gibson, and D. A. Smith, MRS Symposia Proceedings No. 94 (Materials Research Society, Pittsburgh, 1987).

<sup>2</sup> H. Brune, *Surf. Sci. Rep.* **31**, 121 (1998).

<sup>3</sup> I. Meunier, G. Trèglia, J. M. Gray, B. Aufray, and B. Legrand, *Phys. Rev. B* **59**, 10 910 (1999).

<sup>4</sup> C. Kittel, *Introduction to Solid State Physics*, 7th ed. (Wiley, New York, 1996), p. 24.

<sup>5</sup> E. Bauer, *Surf. Sci.* **7**, 351 (1967).

<sup>6</sup> M. Foiles, *Surf. Sci.* **292**, 5 (1993).

<sup>7</sup> J. Jacobsen, L. P. Nielsen, F. Besenbacher, I. Stensgaard, E. Lægsgaard, T. Ramussen, K. W. Jacobsen, and J. K. Nørskov, *Phys. Rev. Lett.* **75**, 489 (1995).

<sup>8</sup> K. Umezawa, S. Nakanishi, and W. M. Gibson, *Phys. Rev. B* **57**, 8842 (1998).

<sup>9</sup> *Low Energy Ion-Surface Interactions*, edited by J. W. Rabalais (Wiley, New York, 1994).

<sup>10</sup> M. Aono, *Nucl. Instrum. Methods Phys. Res. B* **2**, 374 (1984).

<sup>11</sup> G. Molière, *Z. Naturforsch. A* **2A**, 133 (1947).

<sup>12</sup> O. B. Firsov, *Sov. Phys. JETP* **6**, 534 (1958).

<sup>13</sup> R. S. Williams, M. T. Kato, R. S. Daley, and M. Aono, *Surf. Sci.* **225**, 335 (1990).

- <sup>14</sup>K. Umezawa, S. Nakanishi, and W. M. Gibson, *Surf. Sci.* **426**, 225 (1999).
- <sup>15</sup>K. Umezawa, S. Nakanishi, T. Yumura, W. M. Gibson, M. Watanabe, Y. Kido, S. Yamamoto, Y. Aoki, and H. Naramoto,

*Phys. Rev. B* **56**, 10 585 (1997).

- <sup>16</sup>M. Yoshimura, T. An, I. Ono, and K. Ueda, *Surf. Sci.* **433**, 470 (1999).